Carbon 161 (2020) 181–189

Contents lists available at ScienceDirect

Carbon

journal homepage: www.elsevier.com/locate/carbon

Raman spectroscopy analysis of number of layers in mass-produced graphene flakes

Diego L. Silva [a], João Luiz E. Campos [a], Thales F.D. Fernandes [a], Jeronimo N. Rocha [b], Lucas R.P. Machado [b], Eder M. Soares [a], Douglas R. Miquita [d], Hudson Miranda [c], Cassiano Rabelo [c], Omar P. Vilela Neto [b], Ado Jorio [a], Luiz Gustavo Cançado [a, *]

[a] Departamento de Física, Universidade Federal de Minas Gerais, Belo Horizonte, MG, 30123-970, Brazil
[b] Departamento de Ciência da Computação, Universidade Federal de Minas Gerais, Belo Horizonte, MG, 30123-970, Brazil
[c] Programa de Pós-Graduação Em Engenharia Elétrica, Universidade Federal de Minas Gerais, Belo Horizonte, MG, 31270-901, Brazil
[d] Centro de Microscopia, Universidade Federal de Minas Gerais, Belo Horizonte, MG, 31270-901, Brazil

ARTICLE INFO

Article history:
Received 23 October 2019
Received in revised form
16 January 2020
Accepted 16 January 2020
Available online 21 January 2020

ABSTRACT

A metrological framework for statistical analysis of number of layers and stacking order in mass-produced graphene using Raman spectroscopy is presented. The method is based on two complementary protocols, denominated by 2D and G. The 2D–protocol is based on the parameterized principal component analysis of the two-phonon 2D band, and it measures interlayer coupling. A neural-network algorithm for spectral denoising was also developed to improve the outcome. The G–protocol explores the intensity of the bond-stretching G band, and provides information about the number of layers. The method is suitable for automated statistical analysis of heterogeneous graphene-based systems with relatively low computational cost, as shown here for graphene flakes prepared by the liquid-phase exfoliation of graphite.

1. Introduction

With the advent of graphene production in large scale, the development of versatile methods that allow prompt statistical characterization becomes a crucial step towards quality. The measurement of the number of stacked layers, *N*, is one of the most important items in the characterization process of graphene samples [1,2]. These measurements can be performed through different techniques such as optical contrast [3–6], atomic force microscopy (AFM) [7–9], photoelectron emission electron microscopy (PEEM) [10], spin Hall effect (SHE) of light [11], light absorption [12], and Raman spectroscopy [4,6,13–30].

So far, the most common technique used for identifying the number of layers, *N*, is Raman spectroscopy. The measurements can be performed by three distinct routes: (i) the intensity of the G band, occurring at 1580 cm^{-1} and associated with the C–C bond stretching mode [4,6,18,19,26,27]; (ii) the frequency of the shear vibrational mode [28,29,31–36]; and (iii) the shape of the 2D band, a two-phonon band associated with a totally symmetric transversal optical phonon mode occurring near the corners of the first Brillouin zone [13–24,30]. However, the methods developed up to date have numerous problems, as systematically discussed here, and are not ready to be applied on the quality control of large amounts of material.

This work presents a method based on two complementary protocols, named as 2D– and G–protocols, for the measurement of interlayer coupling and number of layers in graphene systems using Raman spectroscopy. The 2D–protocol is based on the parameterized principal component analysis (PCA) [37] of the 2D band's frequency and shape. In the case of the G–protocol, the information about the number of layers is linked to the G band intensity. Combined, they provide a robust method to determine statistical distributions on the number of layers and the degree of interlayer coupling in heterogeneous systems. A semi-automated framework was developed for the simultaneous analysis and quantification of thousands of graphene flakes prepared by the liquid-phase exfoliation of graphite, showing that the method is suitable for the analysis of mass-produced graphene flakes.

* Corresponding author.
E-mail address: cancado@fisica.ufmg.br (L.G. Cançado).

https://doi.org/10.1016/j.carbon.2020.01.050
0008-6223/

2. Experimental details

2.1. Standard samples

The standard graphene samples were produced by mechanical exfoliation of natural graphite, using the "scotch tape" method [38]. Fig. 1 provides an example of how the standard samples were produced and characterized. In Fig. 1 (a), an optical microscopy image of a representative graphene sample sitting on a Si substrate covered with a 90 nm thick SiO_2 layer is presented. The optical contrast clearly shows that the flake has several plateaus with distinct numbers of layers. It is important to produce samples whose plateaus have relatively large area (at least a few micrometers wide) to avoid edge effects in the Raman spectrum. Fig. 1(b) shows a Raman map acquired in the same area shown in Fig. 1(a). The measurement was performed using a Witec imaging system, model alpha 3000, with a 532 nm excitation laser source with superficial power density of $\approx 10^5$ W/cm^2. The color scale renders the G band intensity.

Fig. 1(c) shows an AFM image obtained from the same area as shown in panels 1 (a,b). The measurement was performed using a Park instrument, model NX10, in contact mode, using a HQ:NSC36/Al-Bs tip. As for the Raman case, the determination of numbers of layers by AFM is not trivial. The process is influenced by a wide range of factors, such as the scanning mode [7,39], the type of forces involved [8], and the substrate [9]. The relative height between two plateaus can be precisely measured and the result must be a multiple of the separation distance between two adjacent graphene layers (~ 0.335 nm) [40]. On the other hand, the value obtained for the height of a single monolayer flake ranges from 0.4 to 1.7 nm [8]. The difference lies in the distinct forces involved between the tip and the substrate supporting the graphene, which depends on the tip's type, the substrate's type, the presence or not of contaminants, and the scanning mode [7]. For this reason, the first step in our procedure was to identify a monolayer piece by Raman spectroscopy (2D band's shape). This piece then serves as a base reference for other pieces nearby. To make sure this procedure works properly, we search for a step-like structure as the one shown in Fig. 1, in which the lowest step is formed by a monolayer flake (as identified from the 2D band's shape). The number of layers of the thicker plateaus (adjacent steps) are determined by AFM, considering the relative heights between adjacent plateaus. For example, by following incremental steps like this, the plateaus marked with the characters **a**, **b**, **c**, **d**, and **e** in Fig. 1 were addressed with one, two, six, seven and eight stacked graphene layers, respectively.

2.2. Sample preparation for hyperspectral Raman mapping

The heterogeneous graphene-based sample preparation is a critical step for hyperspectral Raman mapping. The graphene flakes must be spread over a flat and clean surface in such a way that they are not too far from each other, to guarantee the statistical character of the measurement, and not too close, to avoid stacking. The first step to achieve this goal is to functionalize a clean SiO_2/Si substrate to guarantee that a large number of graphene flakes with different thicknesses and lateral sizes stick on it. The process starts with the preparation of an aqueous solution of (3–Aminopropyl)triethoxysilane (APTES) with a 1:40 dilution in DI water. The SiO_2/Si substrate is dipped into the solution for approximately 15 min, to grow a thin layer of APTES over its surface. The APTES functionalizes the SiO_2 surface in order to enhance the adherence of the graphene flakes on it. This is important to avoid agglomeration and/or superposition of flakes. Afterwards, the substrate is rinsed with DI water and dried with a N_2 blow. This process must be repeated 5 times. Once the substrate is properly functionalized, the graphene solution is dropped and spread over the entire SiO_2 surface. The optimal waiting time for the flakes to stick on the substrate depends on the graphene concentration, being $\approx$10 s for $\approx$1 g/L, and $\approx$2 min for $\leq$ 0.1 g/L. Finally, the substrate is again wiped with DI water and dried with a N_2 blow for 5 times.

3. The 2D–protocol

Fig. 2 shows representative 2D band spectra obtained from standard graphene samples (section 2.1) with distinct numbers of stacked layers, as indicated by the numbers written in the top-right corner of each panel (the details on how these numbers were measured are explained in section 2.1). The abbreviation HOPG stands for highly oriented pyrolytic graphite. The graphics clearly show the differences in the 2D band shape for different numbers of layers. Anyone could easily point out the spectrum obtained from monolayer graphene, for which the 2D band presents a symmetric Lorentzian shape. An expert may be able to point out the differences between the 2D band obtained from few-layer (2–5 layers), multi-layer (6–10 layers), and above (more than 10 layers up to graphite). Although these differences are visually clear by comparison, a systematic fitting procedure that allows one to identify the exact features that generate them is not trivial [30]. An excellent example is given in Ref. [41], which describes the complexity of the mechanism giving rise to the 2D band in bilayer graphene. This type of fitting analysis becomes unpracticable for heterogeneous

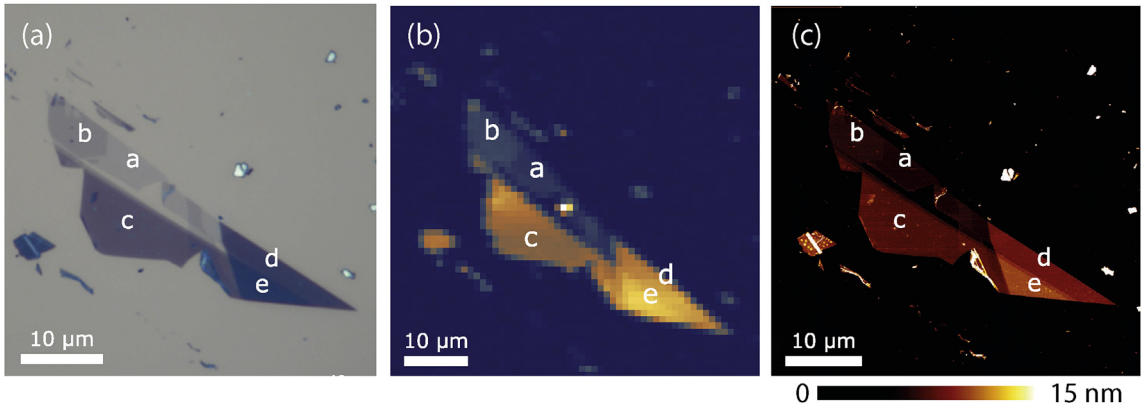

Fig. 1. (a) Optical microscopy image of a representative graphene sample sitting on a Si substrate covered with a 90 nm thick SiO_2 layer. (b) Raman map acquired in the same area shown in panel (a). The color scale renders the intensity of the bond-stretching G-mode, occurring at ~ 1580 cm^{-1}. (c) AFM image obtained from the same area as shown in panels (a,b). (A colour version of this figure can be viewed online.)

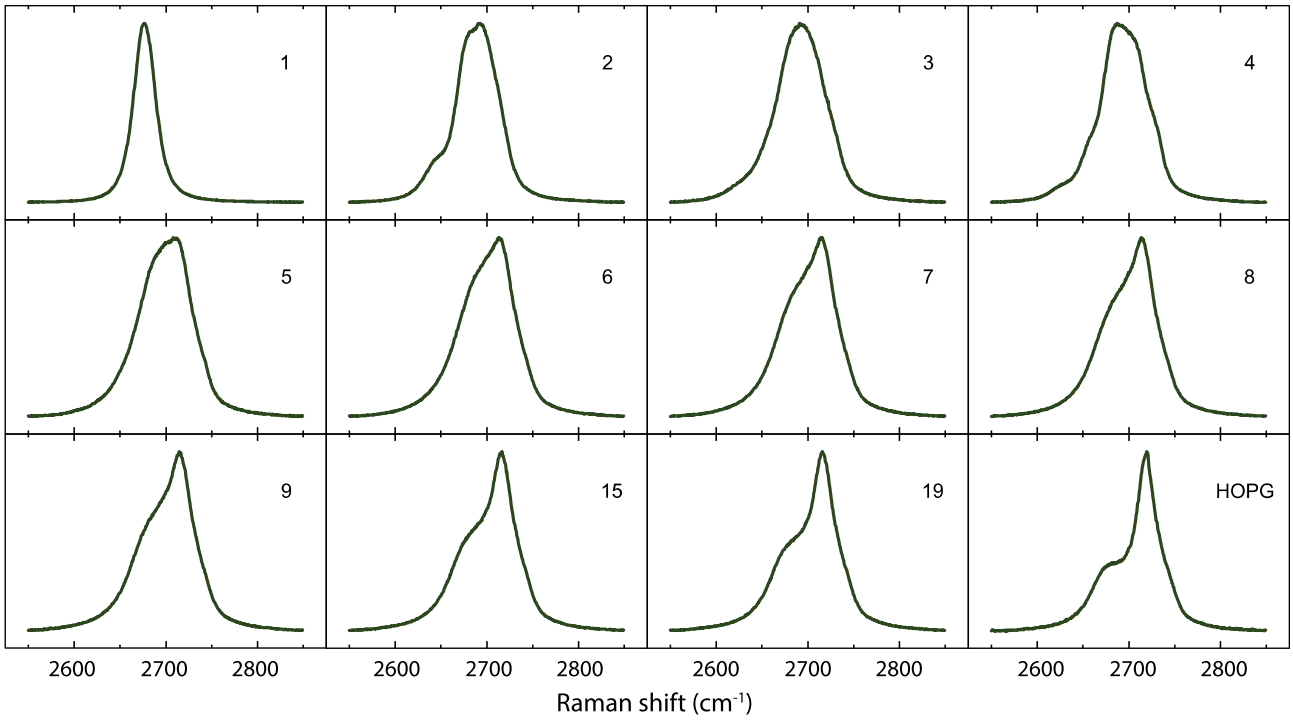

Fig. 2. Representative 2D band spectra obtained from standard graphene samples with distinct numbers of stacked layers *N*, as indicated by the number in the top-right of each panel. The experimental determination of *N* was discussed in section 2.1. The abbreviation HOPG stands for highly oriented pyrolytic graphite. The measurements were performed using a 532 nm excitation laser line. (A colour version of this figure can be viewed online.)

systems such as graphene powders or aqueous solutions, for which robust characterization requires statistical treatment [1,2].

The parameterized PCA algorithm employed here has the same basic groundwork as the method introduced in Ref. [37]. In the parameterized PCA, a subspace is defined by considering the most relevant principal components (PCs) extracted from the Raman spectra obtained from the set of standard samples. In the present case, these samples are mechanically exfoliated pristine graphene flakes whose numbers of stacked layers were previously determined by a combination of optical microscopy, AFM, and Raman spectroscopy measurements. The detailed procedure is presented in section 2.1. Once the number of layers of a given standard sample is determined, its Raman spectrum is measured and the 2D band is recorded as a tagged template. Representative spectra obtained from standard samples (with distinct numbers of layers) were shown in Fig. 2. Before being analysed by the PCA algorithm, the 2D band undergoes a linear baseline subtraction, followed by an intensity normalization which turns its maximum amplitude into unity.

The PCA algorithm starts with the construction of a $n \times m$ matrix in which the elements are recorded spectral intensities. The lines correspond to sample spectra, and the columns correspond to wavenumbers. The coordinate space undergoes a transformation that defines a new basis composed of principal components PC*i*, with $i = 1, 2, \ldots, m$. The experimental data is then rewritten on this new basis in such a way that each experimental data is described as a linear combination of the principal components. The output PCs are written in spectral forms carrying spectral features that enriches minimal variations related to specific properties of the sample, being more sensitive than the original spectra [37].

Similar spectra as the ones shown in Fig. 2 were analysed by PCA, and the results are shown in Fig. 3. It is important to notice that, due to differences in the double-resonance process giving rise to the 2D band, its frequency and shape strongly depends on the excitation laser line [24]. For this reason, the comparison between different samples by PCA is only possible for data obtained with the same excitation laser energy. In the current work we have measured the same standard samples with three distinct laser wavelengths, namely 458, 532, and 633 nm, and the results are shown in Fig. 3(a), 3(b), and 3(c), respectively. Each graph shows a two-dimensional map whose coordinates are the first two principal components. Our analysis show that ≈98% of all spectral information contained in the 2D band can be decomposed in these first two components, named here as PC1 and PC2. Therefore, the two-dimensional plot of PC1 *vs.* PC2 represents a phase space that defines the main spectral features of the 2D band. Since the shape of the 2D band strongly depends on the number of layers, Raman data obtained from samples with different number of layers may dwell different locations in this phase space.

Each data point in Fig. 3(a), (b), and 3(c) represents the result obtained from the PCA algorithm performed on the 2D band spectrum extracted from a specific standard sample. Data obtained from samples with same number of layers are represented with the same color (the number of stacked layers associated with each group is indicated in the graph). It is interesting to observe how the evolution with the number of layers follows a well defined trajectory in the phase diagram. Although distinct groups are easily distinguishable, the data points belonging to a specific group also present some degree of dispersion. This dispersion is specially important for the monolayer, and may be attributed to frequency variations due to strain and/or doping [42,43]. Besides, the dispersion is more evident along the PC2 component, which suggest that this component is susceptible to the 2D band's frequency.

The phase space defined by the set of standard samples maximizes the variances among their Raman spectra. In the parameterized PCA, the same process of orthogonal linear transformation established for the standard samples can be performed over spectra obtained from "real samples" (samples to be characterized). In another words, once the parameterized phase space is determined,

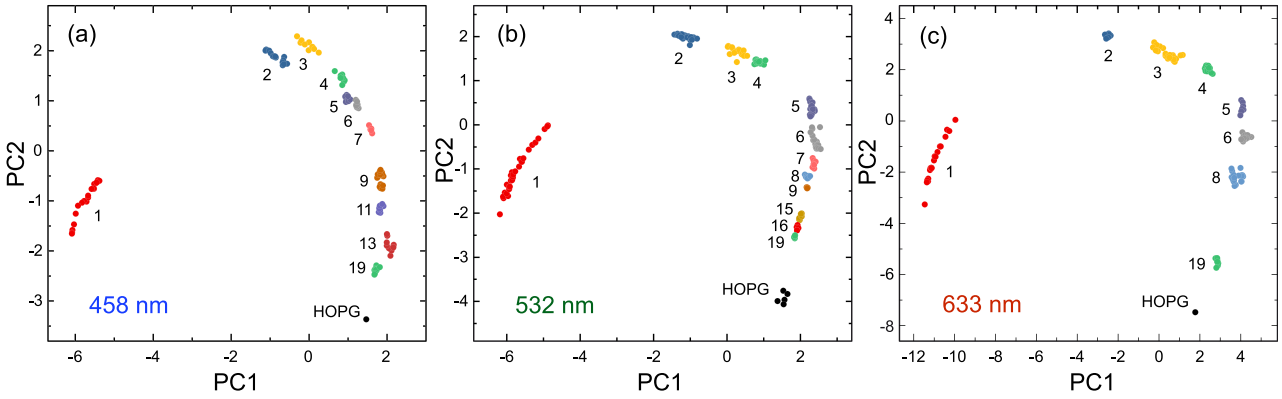

Fig. 3. (a,b,c) Plot of the first two principal components, namely PC1 and PC2, related to Raman spectra extracted from standard graphene samples. Data with same color were obtained from samples with same number of stacked layers, *N* (the number is indicated near each respective group). Panels (a), (b) and (c) show data obtained using 458, 532, and 633 nm excitation laser wavelengths, respectively. HOPG stands for highly oriented pyrolytic graphite. (A colour version of this figure can be viewed online.)

any additional data can be projected onto this phase space to be classified according to its relative location. The classification process can be performed in numerous ways. In the current case, better results were achieved by defining a discrete probability function as follows. The phase space is decorated with *m* groups of standard samples. Each group is associated with a given number of layers, *N*. The quantity P_{ij} that gives the relative probability that a real sample *i* is associated with a specific standard group *j* is defined as

$$P_{ij} = \frac{d_{ij}^{n}}{\sum_{k=1}^{m} d_{ik}^{n}} \tag{1}$$

where d_{ij} is the "distance" (in the PC's phase space) between the projection of the data extracted from sample *i* and the center of a group of data extracted from standard samples classified by the index *j*. $n \leq 1$ is a factor that penalizes the contribution from distant groups. The distance d_{ij} is weighted by the sum in the denominator of Eq. (1), which adds together the distances between the data extracted from sample *i* and the center of all *m* groups of data extracted from the standard samples. Based on the computed probability and a pre-defined confidence interval, we can associate, within a certain level of certainty, each spectrum with a certain number *N*.

4. The G–protocol

Previous works have explored the dependence of the G band intensity on the number of layers in graphene, few–layers graphene, multi–layer graphene and graphite [4,6,18,19,26,27]. Usually, the G band intensity increases monotonically with *N* for flakes with $N \leq 10$ which, according to the International Standards Organization, are considered as graphene [44]. For $N > 10$, the G–intensity drastically drops [18,26], being comparable to the intensity obtained from monolayer graphene for $N \approx 150$ and above [26]. In this case, the same intensity can be obtained for two samples with distinct *N*'s (one with $N < 10$, the other with $N > 10$). In Ref. [6], a HOPG was used as a reference material. For that, the intensity of the G band obtained from graphene samples with $N \leq 5$ was normalized by considering the G band intensity in the Raman spectrum of HOPG. However, this calibration method has drawbacks. First, the aforementioned ambiguity for $N < 10$ and $N > 10$ remains. Second, the reference signal comes from a different sample (the HOPG crystal), obtained in a distinct experiment. Ideally, the reference signal should be present in the same spectrum as the measured signal.

The G–protocol presented here takes the Raman intensity from the SiO_2/Si substrate underneath as a reference signal. Fig. 4(a) shows representative spectra obtained from standard graphene samples with distinct numbers of layers *N*, as indicated for each spectrum. The reference samples are the same as used for the 2D–protocol. Details about their preparation and determination of the number of layers are explained in section 2.1. The Raman spectroscopy measurements were performed using a 532 nm excitation laser line, and the thickness of the SiO_2 layer on the Si substrate was 90 nm. All spectra in Fig. 4(a) were normalized in such a way that the G band is visualized with the same apparent intensity for all of them. In this picture, it is easy to see how the Raman signal from the Si substrate, at $\approx 920\ cm^{-1}$ [45], becomes weaker if compared to the G band signal as the *N* increases. The reason is that, due to the backscattering geometry used in the experiment, both incident and scattered fields on and from the Si substrate, respectively, are blocked by the graphene piece atop. Fig. 4(b) shows the plot of the ratio between the G band intensity, I_G, and the Raman signal from the Si substrate, I_{Si}, as a function of *N*. As shown in the graphics, although the relation becomes highly nonlinear for $N > 10$, all values of I_G/I_{Si} for $N > 10$ overcome the value obtained for $N = 10$. In other words, the $N < 10$ vs. $N > 10$ ambiguity is surmounted.

The dependency of the I_G/I_{Si} ratio on *N* has a monotonic trend for $N \leq 10$, as shown Fig. 4(c), which is a magnification of the blue-boxed area in Fig. 4(b). The bullets are the experimental points, and the dashed line is a fit according to the empirical relation

$$I_G \Big/ I_{Si} = a + \frac{b-a}{1+(N/c)^2}\ , \tag{2}$$

with the fitting parameters $a = 20.7$, $b = 0.6$, and $c = 11$. There are three important details to be noticed. First, because I_G strongly depend on the thickness of the SiO_2 layer, the fitting parameters (*a*, *b*, and *c*) obtained here are only valid for samples sitting on SiO_2/Si substrates whose SiO_2 layer is 90 nm thick. Second, the fitting parameters obtained here are only valid for experimental data obtained with a 532 nm laser line. Third, Equation (2) is only valid for $N \leq 10$ (graphene).

Each rectangular box in Fig. 4(c) is related to a given *N*, and its length is equal to 1. If the I_G/I_{Si} value of a given sample falls in a box centered at an specific *N*, the sample will be tagged as a graphene with *N* layers. If the I_G/I_{Si} ration is larger than the values defined by the box centered at $N = 10$, the sample will be tagged as a graphite piece.

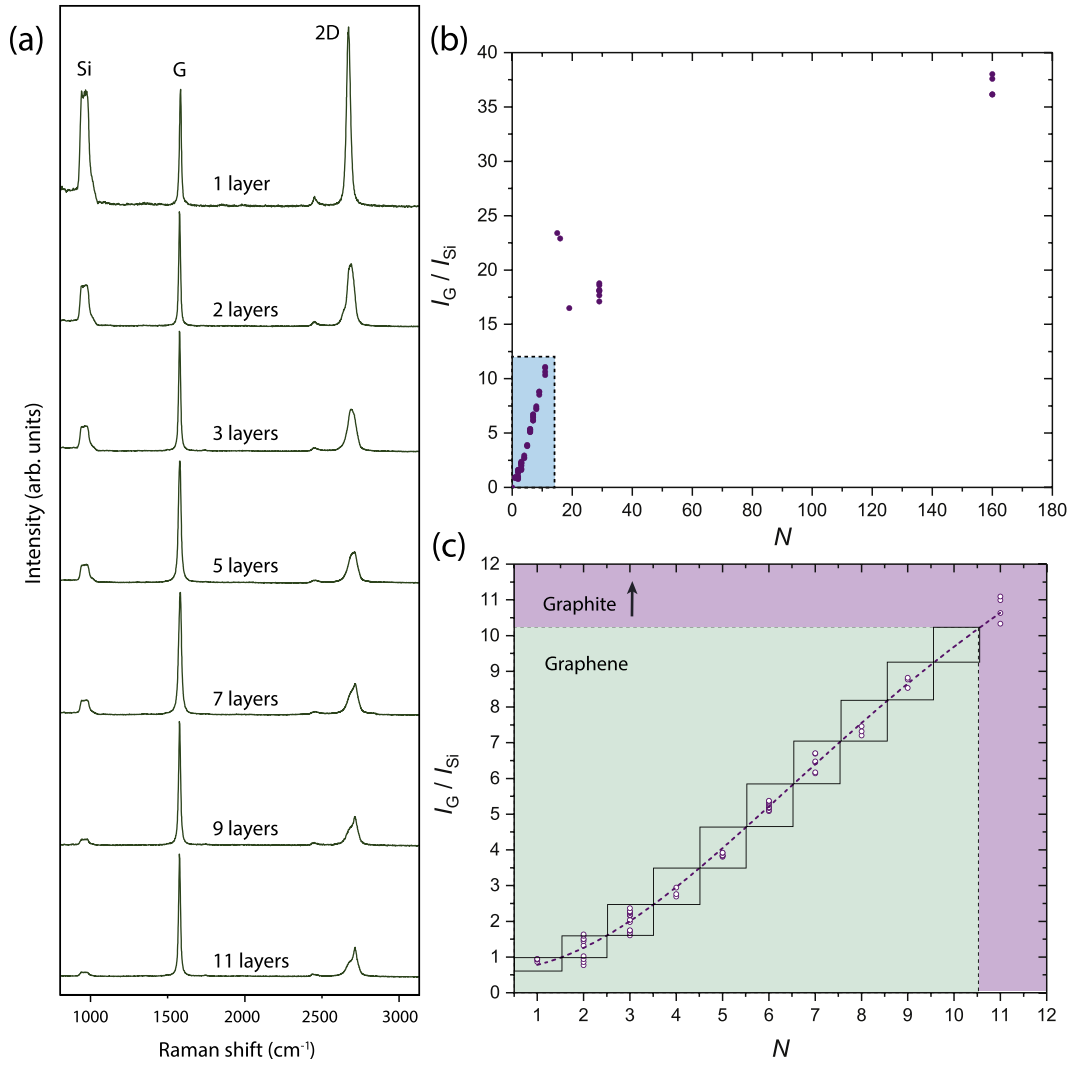

Fig. 4. (a) Representative spectra obtained from standard graphene samples with distinct numbers of stacked layers *N*, as indicated by the number on the top of each spectrum. The determination of *N* was made following the PCA analysis of the 2D band. The measurements were performed using a 532 nm excitation laser line. (b) Plot of the experimental data obtained for the ratio between the G band intensity, I_G, and the Raman signal from the Si substrate, I_{Si}, as a function of *N*. (c) Magnification of the blue-boxed area in panel (b). The bullets are the experimental points, and the dashed line is a fit according to Eq. (2). Each rectangular box defines the range of I_G/I_{Si} values that should be assigned to the respective *N*. (A colour version of this figure can be viewed online.)

5. Case study: statistical analysis of liquid-phase exfoliated graphene flakes

One of the most important advantages of using the 2D– and G–protocols is the possibility of classifying large amounts of data with relatively low computational cost. To illustrate this capability, we have characterized a graphene sample produced by liquid-phase exfoliation (LPE) of natural graphite [12,46]. In this process, the separation of graphene from the remaining micronized graphite is attained by centrifugation. The 2D– and G–protocols were performed over hyperspectral Raman maps of several thousands of individual flakes spread out over a flat APTES-functionalized SiO_2/Si substrate with 90 nm of SiO_2–thickness (see details about sample preparation in section 2.2). The Raman maps covered 10 μm × 10 μm areas, in steps of 100 nm. Each spectrum was taken within 0.1 s of accumulation time, and the superficial power density of the 532 nm laser line was kept at ≈ 10^5 W/cm^2 to avoid sample heating.

Fig. 5(a) shows the plot of the PC2 *vs.* PC1 components describing the 2D band. Each green data point corresponds to a single spectrum extracted from the hyperspectral Raman map of the LPE sample. The red bullets indicate the center of mass of each group of data points plotted in Fig. 3(b) (corresponding to specific *N* values), for reference. The output data obtained from this rough PCA analysis is spread over the PCA phase-space, and barely follows the trajectory defined by the standard samples. As shown in the next lines, the reason for this diffused aspect is the low signal-to-noise ratio usually present in Raman spectra obtained from hyperspectral maps.

The spectra contained in the hyperspectral Raman maps of liquid exfoliated graphene present low signal-to-noise ratio due to the short accumulation time (1 s or less) and relatively low laser power density. This low signal-to-noise ratio jeopardizes the PCA analysis, since the shape of the 2D band is unresolved. As shown in Fig. 5(a), the poor quality of the collected spectra deviates their projection on the PCA phase space from the trajectory defined by the standard samples (red bullets). Increasing the accumulation time is unpractical for many reasons, the most effective being thermal drift that generates defocusing. Raising the incident laser power density is not an option either, due to the risk of sample

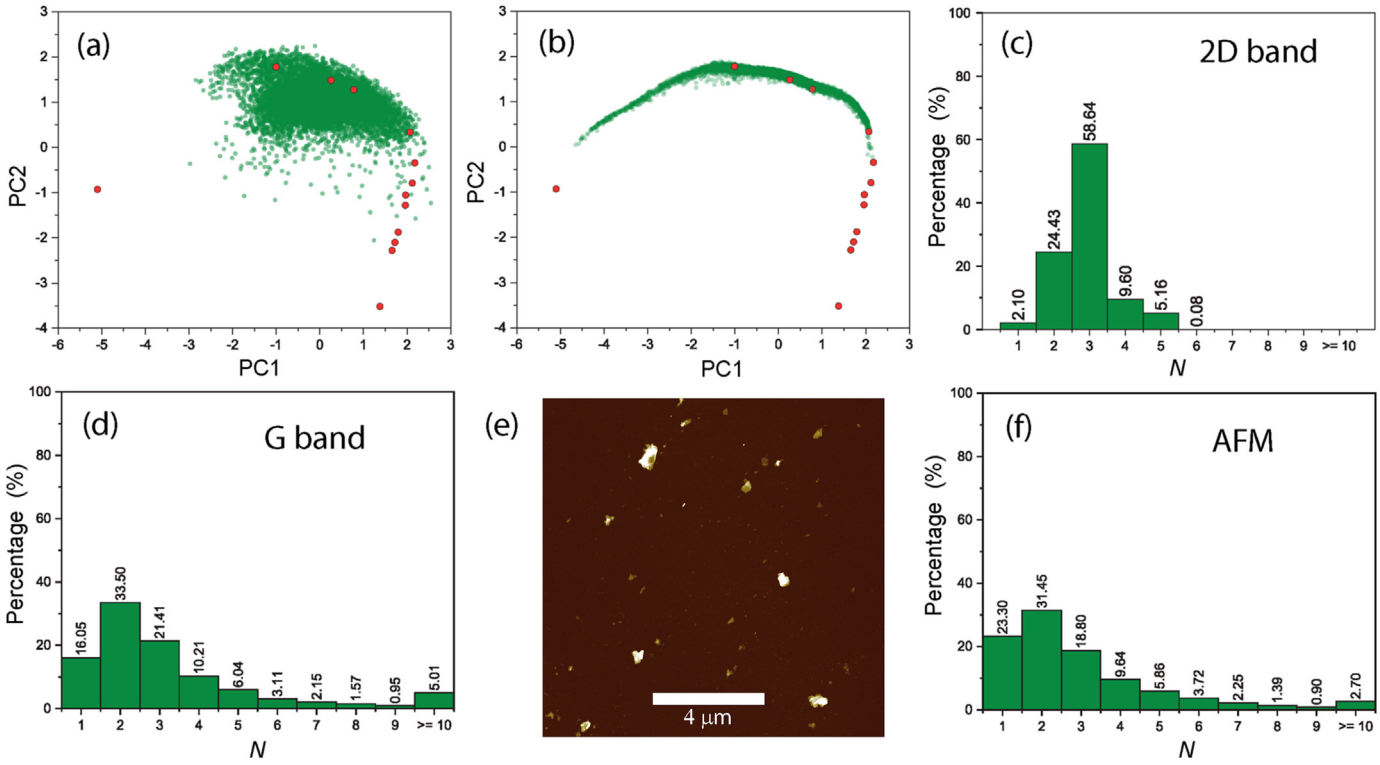

Fig. 5. (a) Plot of PC2 *vs*. PC1 components describing the 2D band data extracted from a sample produced by liquid-phase exfoliation of natural graphite. Each green data point corresponds to a single spectrum extracted from a hyperspectral Raman map. The red bullets indicate the center of mass of each group of data points plotted in Fig. 3(b) (corresponding to specific *N* values), for reference. (b) Result of the PCA analysis performed over the same experimental data as in panel (a), but after applying the neural network denoising algorithm. (c) Histogram describing the statistical distribution of the number of layers, obtained from the output of the 2D−protocol presented in panel (b). (d) Histogram describing the statistical distribution of the number of layers, obtained from the G−protocol. (e) AFM image of the sample. (f) Histogram describing the statistical distribution of the number of layers, extracted from an AFM image of the same area scanned in the Raman mapping procedure that gave rise to the data shown in panels (c,d). (A colour version of this figure can be viewed online.)

burning. In order to overcome this difficulty, we have developed a denoising process based on a neural network algorithm.

The neural network architecture is a convolutional auto-encoder that revolves around a training model to reduce the dimensionality of the input data [47–50]. In short, noise cannot pass through an algorithm that uses compressed data to build the processed output, because it cannot be compressed effectively. Instead of using two-dimensional operations as for image processing, temporal convolutional layers (one-dimensional convolution) were used in the present case since our data (2D band spectra) are one dimensional. The training was performed using two different types of data. First, low-noise spectra obtained from the standard samples were used as background data. Second, a database composed of spectra obtained with different accumulation times was built, yielding for different levels of noise. A certain level of pure noise was then gathered by subtracting a spectrum with a given accumulation time from the low-noise spectrum. With pure noise and low-noise spectra in hands, we were able to generate large amounts of training data to fit our model. After training, the model was tested by measuring the distance from the denoised data to the original standard data in the PCA phase-space. The outcome is presented in Fig. 5(b), which shows the result of the PCA analysis performed over the same experimental data as in Fig. 5(a), but after applying the neural network denoising algorithm. The comparison between the two graphics shown in Fig. 5(a) and (b) demonstrates great improvement, with the denoised data following the trajectory defined by the standard samples (red bullets) in Fig. 5(b). Fig. 5(c) shows the histogram describing the statistical distribution of the number of layers, obtained from the indexation process based on the 2D−protocol. According to the parameterized PCA analysis of the 2D band, the great majority of the measured flakes were classified to be in the range between two- and five-layers, with the mode at $N = 3$.

Fig. 5(d) shows the plot of the histogram describing the statistical distribution of the number of layers, obtained from the G−protocol. According to this analysis, the graphene flakes are distributed from $N = 1$ to $N = 10$, with the mode at $N = 2$, and a considerable amount ($\approx$5%) of flakes were classified as graphite ($N > 10$). This result is strikingly different from the result provided by the 2D−protocol, specially considering the population of graphite pieces, not detected by the 2D−protocol. In fact, 5% of graphite in a population distribution corresponds to a significative amount of mass (more than 90%), and cannot be neglected. Another important difference is the percentage of monolayer graphene flakes − while the G− protocol indicates 16%, the 2D− protocol barely detected their presence. This issue is discussed in section 6.

Tens of similar experiments were performed in LPE samples, and the differences in the results obtained by the 2D− and G−protocols [presented in Fig. 5(c and d)] were observed in most of them. In order to understand the origin of these discrepancies, an AFM topographic image was obtained over the same area where the Raman maps were taken. The AFM image, shown in Fig. 5(e), was performed over the 10 μm × 10 μm area in steps of 1 nm, in conventional intermittent contact mode. The population histogram as a function of *N* obtained by AFM is shown in Fig. 5(f). The similarity with the results obtained by the G−protocol is evident, indicating that the G−protocol provides statistically faithful information about the morphology of the flakes. This result is physically sound,

since the I_G/I_{Si} ratio scales with the thickness of the flake, as shown in Fig. 4.

The fact that the results obtained from the 2D−protocol do not match with the AFM results indicates that the 2D band does not necessarily reflect the morphology of flakes. Unlike the G−protocol, the 2D− protocol is not based on signal strength, but on the shape of the 2D band that, in turn, is sensitive to changes in the electronic and vibrational structures of graphene and graphite flakes due to the coupling between adjacent layers. Therefore, the 2D−protocol delivers valuable information on the degree of interlayer coupling which does not necessarily reflect the number of layers. The 2D band's shape can only be directly translated to N if all adjacent layers are electronically bound. In other words, the 2D−protocol measures interlayer coupling in the presence of perfect AA− or AB-stacking, but is not able to probe the morphology of turbostractic structures in which the staking order fails. Perfect stacking is distinct from disordered piling, and the difference is commonly neglected in this type of analysis. An illustrative example is given in Fig. 6(a), which shows a transmission electron microscopy (TEM) image of a graphene flake extracted from the LPE sample. The definition of the exact number of layers in this structure is not clear. There are inhomogeneities all over the flake, and it is not possible to allege if the variations are due to folding or different numbers of layers. Fig. 6(b) shows a magnification of the boxed area in Fig. 6(a). From this image one can clearly see that, although there is a stacking, some of the adjacent planes are uncoupled. The G− and 2D−protocols would certainly provide distinct and complementary types of information about this flake.

Fig. 7 shows a Raman spectrum obtained directly from the calcinated LPE powder. The comparison of this spectrum with the spectra shown in Fig. 2 (visual inspection of the 2D band shape) indicates that most of the graphene content in this sample may have an average number of layers of 5. This conclusion is supported by the application of the 2D−protocol on this specific spectrum,

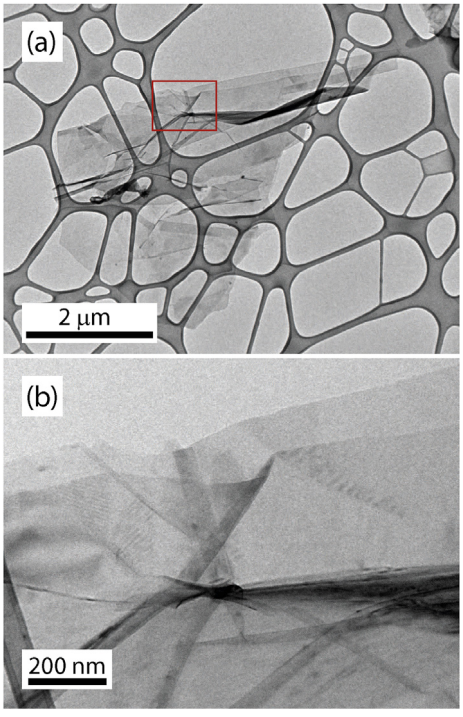

Fig. 6. (a) Transmission electron microscopy (TEM) image of a graphene flake extracted from the LPE sample. (b) Magnification of the boxed area in panel (a). (A colour version of this figure can be viewed online.)

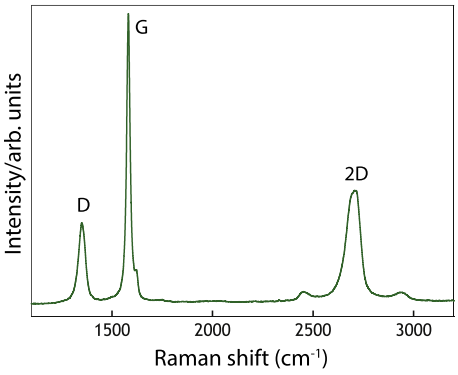

Fig. 7. Raman spectrum extracted directly from the calcinated LPE powder. (A colour version of this figure can be viewed online.)

which gives $N = 5$. However, $N = 3$ gives the mode of the histogram of population shown in Fig. 5(c), obtained by the application of the 2D−protocol over thousands of individual flakes extracted from the LPE solution. These results show that great care should be taken when analysing the number of layers by considering the 2D band's shape alone.

6. Limitations

In this section we enumerate the limitations found during the application of the 2D− and G−protocols.

- Although the G−protocol is useful to detect distinct numbers of layers composing distinct plateaus coexisting in the same sample, the absolute number of layers of each plateau is still uncertain, unless a monolayer plateau is present to serve as a reference for the least intensity unity. This issue is attenuated by the fact that monolayer graphene pieces can be easily identified by the single lorentzian shape of the 2D band. However, the 2D peak becomes broader as the amount of defects increases [22]. In this case, the PCA analysis can be compromised because the 2D band obtained from defective monolayer flake can be as broad as the 2D band obtained from few-layer graphene. These issues could be the reason why the G− and 2D−protocols do not agree about the number of monolayer graphene flakes in the measurement of the LPE sample (Fig. 5).
- If the graphene sample is sitting on a SiO_2/Si substrate, as usual, the G intensity strongly depends on the thickness of the SiO_2 layer [6].
- When the graphene flakes have lateral sizes shorter than the diameter of the incident laser spot at the focal plane, the fitting curve shown in Fig. 4(c) [Eq. (2)] must be re-scaled with the help of the 2D−protocol. For that, a large amount (at least hundreds) of flakes should be measured, and the pieces classified with $N = 2$ (according to the 2D−protocol) with a confidence interval wider than 90% are considered as two-layer graphene. The vertical scale in the graphics of I_G/I_{Si} vs. N is then re-scaled in such a way that the average value of the I_G/I_{Si} ratio obtained from the selected flakes falls in the center of the rectangular box assigned to $N = 2$. This procedure was successfully applied on liquid-phase exfoliated graphene samples, as reported in the last section. It is important to notice that, if the flake is shorter than the diameter of the incident laser spot at the focal plane, the I_G/I_{Si} will present distinct values for data obtained using objective lenses with different numerical apertures (NA). For this reason, all data should be collected with the same objective lens used to measure the standard samples.

- Both 2D– and G–protocols have uncertainties related to the possibility of occurrence of two or more pieces with different numbers of layers inside the incident laser spot area. In this case, and average value of *N*, weighted by the area of each piece, should be obtained from the G–protocol. For the 2D protocol, the 2D band may assume a broad shape that will probably be classified with *N* between 2 and 5. For instance, we prepare the samples in such a way that most flakes are detached from each other and spread over the substrate surface (see detailed procedure in section 2.2). However, there is no guarantee that the problem does not occur. We are currently investigating different ways to perform the disentanglement of the information coming from different flakes inside the same laser spot area, and the results shall be presented in a future work.
- The G– and 2D-protocols presented here account for AB-stacked graphene flakes. The occurrence of ABC stacking or twisted stacking cannot be ruled out, and the model could fail in such cases.

7. Conclusion

The state-of-the-art in terms of statistical analysis of number of layers and stacking order in graphene flakes using Raman spectroscopy was presented. The metrological framework is specially important for mass–produced graphene. Specific parameterized PCA and neural-network algorithm for spectral denoising were developed and utilized. The method is based on two complementary protocols, named as 2D– and G–protocols, for the measurement of interlayer coupling and number of layers, respectively. Both protocols have particular merits and limitations, making them complementary to each other. The 2D–protocol provides information about interlayer coupling, but fails on providing accurate information about the morphology of the flakes. The G–protocol provides information about the morphology of the flakes, similar to an AFM analysis, but is insensitive to the degree of interlayer coupling between adjacent layers. When combined, these protocols provide a method to infer the degree of interlayer coupling and number of layers of heterogeneous systems such as graphene powders or aqueous solutions, for which robust characterization requires statistical treatment and automatization.

CRediT authorship contribution statement

Diego L. Silva: Data curation, Formal analysis, Writing - review & editing, Investigation, Methodology. **João Luiz E. Campos:** Data curation, Formal analysis, Writing - review & editing, Investigation, Methodology. **Thales F.D. Fernandes:** Data curation, Formal analysis, Writing - review & editing, Investigation, Methodology. **Jeronimo N. Rocha:** Software, Formal analysis. **Lucas R.P. Machado:** Software, Formal analysis. **Eder M. Soares:** Data curation, Methodology. **Douglas R. Miquita:** Data curation, Formal analysis, Investigation, Methodology. **Hudson Miranda:** Formal analysis, Investigation, Methodology, Writing - review & editing. **Cassiano Rabelo:** Formal analysis, Investigation, Methodology, Writing - review & editing. **Omar P. Vilela Neto:** Conceptualization, Formal analysis, Funding acquisition, Investigation, Methodology, Resources, Software, Supervision, Validation, Visualization, Writing - review & editing. **Ado Jorio:** Formal analysis, Funding acquisition, Investigation, Methodology, Resources, Validation, Writing - review & editing. **Luiz Gustavo Cançado:** Conceptualization, Data curation, Formal analysis, Funding acquisition, Investigation, Methodology, Project administration, Resources, Supervision, Validation, Visualization, Writing - original draft.

Acknowledgements

This work was funded by Companhia de Desenvolvimento de Minas Gerais – CODEMGE - through the MGgrafeno initiative. The authors acknowledge CAPES, CNPq and FAPEMIG. LGC acknowledges INCT Nanocarbono. The Raman measurements were performed at LCPNano - UFMG.

References

[1] A.P. Kauling, A.T. Seefeldt, D.P. Pisoni, R.C. Pradeep, R. Bentini, R.V. Oliveira, et al., The worldwide graphene flake production, Adv. Mater. (2018) 1803784–1803789.
[2] P. Bøggild, The war on fake graphene, Nature (2018) 502–503.
[3] L. Gao, W. Ren, F. Li, H.-M. Cheng, Total color difference for rapid and accurate identification of graphene, ACS Nano 2 (8) (2008) 1625–1633.
[4] Z. Ni, H. Wang, J. Kasim, H. Fan, T. Yu, Y. Wu, et al., Graphene thickness determination using reflection and contrast spectroscopy, Nano Lett. 7 (9) (2007) 2758–2763.
[5] C. Casiraghi, A. Hartschuh, E. Lidorikis, H. Qian, H. Harutyunyan, T. Gokus, et al., Rayleigh imaging of graphene and graphene layers, Nano Lett. 7 (9) (2007) 2711–2717.
[6] M. Bayle, N. Reckinger, A. Felten, P. Landois, O. Lancry, B. Dutertre, et al., Determining the number of layers in few-layer graphene by combining Raman spectroscopy and optical contrast, J. Raman Spectrosc. 49 (1) (2018) 36–45.
[7] P. Nemes-Incze, Z. Osváth, K. Kamarás, L. Biró, Anomalies in thickness measurements of graphene and few layer graphite crystals by tapping mode atomic force microscopy, Carbon 46 (11) (2008) 1435–1442.
[8] C.J. Shearer, A.D. Slattery, A.J. Stapleton, J.G. Shapter, C.T. Gibson, Accurate thickness measurement of graphene, Nanotechnology 27 (12) (2016) 125704–125714.
[9] C.H. Lui, L. Liu, K.F. Mak, G.W. Flynn, T.F. Heinz, Ultraflat graphene, Nature 462 (7271) (2009) 339–341.
[10] H. Hibino, H. Kageshima, M. Kotsugi, F. Maeda, F.-Z. Guo, Y. Watanabe, Dependence of electronic properties of epitaxial few-layer graphene on the number of layers investigated by photoelectron emission microscopy, Phys. Rev. B 79 (12) (2009) 125437–125443.
[11] X. Zhou, X. Ling, H. Luo, S. Wen, Identifying graphene layers via spin hall effect of light, Appl. Phys. Lett. 101 (25) (2012) 251602–251605.
[12] C. Backes, K.R. Paton, D. Hanlon, S. Yuan, M.I. Katsnelson, J. Houston, R.J. Smith, et al., Spectroscopic metrics allow in situ measurement of mean size and thickness of liquid-exfoliated few-layer graphene nanosheets, Nanoscale 8 (7) (2016) 4311–4323.
[13] L. Cançado, K. Takai, T. Enoki, M. Endo, Y. Kim, H. Mizusaki, et al., Measuring the degree of stacking order in graphite by Raman spectroscopy, Carbon 46 (2) (2008) 272–275.
[14] L. Malard, M. Pimenta, G. Dresselhaus, M. Dresselhaus, Raman spectroscopy in graphene, Phys. Rep. 473 (5–6) (2009) 51–87.
[15] A.C. Ferrari, Raman spectroscopy of graphene and graphite: disorder, electron–phonon coupling, doping and nonadiabatic effects, Solid State Commun. 143 (1–2) (2007) 47–57.
[16] A.C. Ferrari, D.M. Basko, Raman spectroscopy as a versatile tool for studying the properties of graphene, Nat. Nanotechnol. 8 (4) (2013) 235–246.
[17] Z. Ni, Y. Wang, T. Yu, Z. Shen, Raman spectroscopy and imaging of graphene, Nano Res. 1 (4) (2008) 273–291.
[18] D. Yoon, H. Moon, H. Cheong, J.S. Choi, J.A. Choi, B.H. Park, Variations in the Raman spectrum as a function of the number of graphene layers, J. Korean Phys. Soc. 55 (3) (2009) 1299–1303.
[19] Y. Hao, Y. Wang, L. Wang, Z. Ni, Z. Wang, R. Wang, et al., Probing layer number and stacking order of few-layer graphene by Raman spectroscopy, Small 6 (2) (2010) 195–200.
[20] A.C. Ferrari, J. Meyer, V. Scardaci, C. Casiraghi, M. Lazzeri, F. Mauri, et al., Raman spectrum of graphene and graphene layers, Phys. Rev. Lett. 97 (18) (2006) 187401–187404.
[21] J. Park, A. Reina, R. Saito, J. Kong, G. Dresselhaus, M. Dresselhaus, G' band Raman spectra of single, double and triple layer graphene, Carbon 47 (5) (2009) 1303–1310.
[22] E.M. Ferreira, M.V. Moutinho, F. Stavale, M. Lucchese, R.B. Capaz, C. Achete, A. Jorio, Evolution of the Raman spectra from single-, few-, and many-layer graphene with increasing disorder, Phys. Rev. B 82 (12) (2010) 125429–125437.
[23] L. Malard, J. Nilsson, D. Elias, J. Brant, F. Plentz, E. Alves, et al., Probing the electronic structure of bilayer graphene by Raman scattering, Phys. Rev. B 76 (20) (2007) 201401–201404.
[24] L. Cançado, A. Reina, J. Kong, M. Dresselhaus, Geometrical approach for the study of g' band in the Raman spectrum of monolayer graphene, bilayer graphene, and bulk graphite, Phys. Rev. B 77 (24) (2008) 245408–245416.
[25] R. Rao, R. Podila, R. Tsuchikawa, J. Katoch, D. Tishler, A.M. Rao, M. Ishigami, Effects of layer stacking on the combination Raman modes in graphene, ACS Nano 5 (3) (2011) 1594–1599.
[26] Y. Wang, Z. Ni, Z. Shen, H. Wang, Y. Wu, Interference enhancement of Raman

signal of graphene, Appl. Phys. Lett. 92 (4) (2008), 043121–043123.
[27] P. Klar, E. Lidorikis, A. Eckmann, I.A. Verzhbitskiy, A. Ferrari, C. Casiraghi, Raman scattering efficiency of graphene, Phys. Rev. B 87 (20) (2013) 205435–205446.
[28] F. Herziger, P. May, J. Maultzsch, Layer-number determination in graphene by out-of-plane phonons, Phys. Rev. B 85 (23) (2012) 235447–235451.
[29] P.H. Tan, W.P. Han, W.J. Zhao, Z.H. Wu, K. Chang, H. Wang, et al., The shear mode of multilayer graphene, Nat. Mater. 12 (2012) 294–300.
[30] L.M. Malard, M.H.D. Guimarães, D.L. Mafra, M.S.C. Mazzoni, A. Jorio, Group-theory analysis of electrons and phonons in *n*-layer graphene systems, Phys. Rev. B 79 (2009) 125426–125433.
[31] J.B. Wu, X. Zhang, M. Ijäs, W.P. Han, X. Fen Qiao, X.L. Li, et al., Resonant Raman spectroscopy of twisted multilayer graphene, Nat. Commun. 5 (2014) 5309.
[32] J.B. Wu, H. Wang, X.L. Li, H. Peng, P.H. Tan, Raman spectroscopic characterization of stacking configuration and interlayer coupling of twisted multilayer graphene grown by chemical vapor deposition, Carbon 110 (2016) 225–231.
[33] M.L. Lin, T. Chen, W. Lu, Q.H. Tan, P. Zhao, H.T. Wang, et al., Identifying the stacking order of multilayer graphene grown by chemical vapor deposition via Raman spectroscopy, J. Raman Spectrosc. 49 (2018) 46–53.
[34] M.L. Lin, J.B. Wu, X.L. Liu, P.H. Tan, Probing the shear and layer breathing modes in multilayer graphene by Raman spectroscopy, J. Raman Spectrosc. 49 (2018) 19–30.
[35] J.B. Wu, M.L. Lin, X. Cong, H.N. Liu, P.H. Tan, Chem. Soc. Rev. 47 (2018) 1822–1873.
[36] X.L. Li, W.P. Han, J.B. Hu, X.F. Qiao, J. Zhang, P.H. Tan, Layer number dependent optical properties of 2D materials and their application for thickness determination, Adv. Funct. Mater. 27 (2017), 1604468.
[37] J.L.E. Campos, H. Miranda, C. Rabelo, E. Sandoz-Rosado, S. Pandey, J. Riikonen, et al., Applications of Raman spectroscopy in graphene-related materials and the development of parameterized pca for large-scale data analysis, J. Raman Spectrosc. 49 (1) (2018) 54–65.
[38] K. Novoselov, D. Jiang, F. Schedin, T. Booth, V. Khotkevich, S. Morozov, A. Geim, Two-dimensional atomic crystals, Proc. Natl. Acad. Sci. 102 (30) (2005) 10451–10453.
[39] T.F. Fernandes, B.R. Neves, Friction coefficient mapping of 2d materials via friction-induced topographic artifact in atomic force microscopy, JAN 1 (2) (2016) 339–341.
[40] M. Dresselhaus, Graphite Fibers and Filaments, Springer Series in Materials Science, Springer-Verlag, 1988.
[41] F. Herziger, M. Calandra, P. Gava, P. May, M. Lazzeri, F. Mauri, J. Maultzsch, Two-dimensional analysis of the double-resonant 2d Raman mode in bilayer graphene, Phys. Rev. Lett. 113 (2014) 187401–187405.
[42] R. Beams, L.G. Cançado, L. Novotny, Raman characterization of defects and dopants in graphene, J. Phys. Condens. Matter 27 (8) (2015), 083002–083028.
[43] D. Yoon, Y.-W. Son, H. Cheong, Strain-dependent splitting of the double-resonance Raman scattering band in graphene, Phys. Rev. Lett. 106 (15) (2011) 155502–155505.
[44] ISO – International Organization for Standardization, Nanotechnologies – Vocabulary – Part 13: Graphene and Related Two-Dimensional (2D) Materials, 2016.
[45] P.A. Temple, C.E. Hathaway, Multiphonon Raman spectrum of silicon, Phys. Rev. B 7 (1973) 3685–3697.
[46] J.N. Coleman, Liquid exfoliation of defect-free graphene, Acc. Chem. Res. 46 (1) (2013) 14–22.
[47] P. Baldi, Autoencoders, unsupervised learning, and deep architectures, J. Mach. Learn. Res. 27 (2012) 37–50.
[48] K. Fukushima, Neural network model for a mechanism of pattern recognition unaffected byshift in position – Neocognitron, Trans. IECE J62–A (10) (1979) 658–665.
[49] Y. LeCun, Y. Bengio, G. Hinton, Deep learning, Nature 521 (2015) 436–444.
[50] P. Vincent, H. Larichelle, Y. Bengio, P.A. Manzagol, Extracting and composing robust features with denoising autoencoders, in: Proceedings of the 25th International Conference on Machine Learning (ICML 08), 2008, pp. 1096–1103.